Cronfa - Swansea University Open Access Repository

_____

This is an author produced version of a paper published in:
Mechanism and Machine Theory

_____

Paper:

_____

http://www.swansea.ac.uk/library/researchsupport/ris-support/

Bidirectional Torsional Negative Stiffness Mechanism for Energy Balancing Systems

Jiaying Zhang[1,*], Alexander D. Shaw[1], Mohammadreza Amoozgar[1],

Michael I. Friswell[1] and Benjamin K.S. Woods[2]

[1] College of Engineering, Swansea University, Swansea SA1 8EN, United Kingdom

[2] Department of Aerospace Engineering, University of Bristol, Bristol BS8 1TR, United Kingdom

[*]E-mail: jiaying.zhang@swansea.ac.uk

Abstract. A new concept of an integrated bidirectional torsional negative stiffness mechanism is introduced which allows for passive energy balancing of mechanical systems by reducing actuation requirements and improving energy efficiency. This novel design is a modular device, is bidirectional and is easily integrated and customised for different applications. The energy balance concept is achieved by employing a negative stiffness system to couple with a positive stiffness system of the mechanical system to create a zero stiffness system which can be driven with lower energy requirements. The bidirectional torsional negative stiffness mechanism proposed here uses a series of pre-compressed springs around a bidirectional torque shaft to convert decreasing force in the springs into increasing torque output through geometric reconfiguration to generate the negative stiffness characteristic. The kinematics of the negative stiffness mechanism were derived and a physical model was assembled from LEGO® components for validation. An analytical model was developed for prediction and the numerical results showed that a satisfactory performance can be generated to match the torque requirements. An experimental demonstrator was then built and tested to verify the predictions from the analysis. To show the impact of the energy balancing concept on actuator efficiency, a representative case study is made of a tendon-driven morphing active camber mechanism. The performance of the optimised bidirectional negative stiffness device is investigated to shows an improvement by the kinematics tailoring.

Keyword. negative stiffness mechanism; bidirectional torsional; kinematics tailoring; energy balancing; actuator efficiency.

1. Introduction

Traditional mechanisms and smart structures are designed by using actuators or smart materials to overcome the internal (e.g. structure deformation) resistance and external (e.g. aerodynamic load) loads to generate motion of the system. Frequently the use of these actuators to drive the system can cost noteworthy energy for each cycle of operation and the spent energy cannot be recovered. Therefore, some concepts have been proposed to reduce the required force or torque and therefore to allow smaller and lighter actuators, or even no actuator, to be employed to drive the system. For some typical cases, such as gravity equilibrators, a weight can be carried throughout its range of motion without any external energy by using spring mechanisms or counterweights [1–3]. Such static balancing is described as "zero stiffness" or "neutral stability", as the system can be moved without operating energy. In general, many systems have force that is purely a function of displacement, as shown in Fig. 1(a), known as an elastic force response. In general, many systems have force that is purely a function of displacement, as shown in Fig. 1(a), known as an elastic force response. In order to produce a static balancing for such system with a zero stiffness property, negative stiffness is required to assist the imposed deformation. Figure 1(b) shows a representative negative stiffness property, which has a completely opposite behaviour to the positive stiffness system and helps to construct an energy balancing system shown in Fig. 1(c). As the actuation is returned to zero, the elastic energy stored in the driven structure will force the negative stiffness system back to its original state, again at zero net actuation force. Therefore, Figure 1 shows that for system assumed to be perfectly elastic, negative stiffness can drive required actuation force to zero. Of course, many real systems include significant inelastic forces, which can be rate or history dependent, or due to external disturbance, and these cases represent a more complex problem that will be the subject of future work. In what follows, it is assumed that the driven structure has a purely elastic force displacement response.
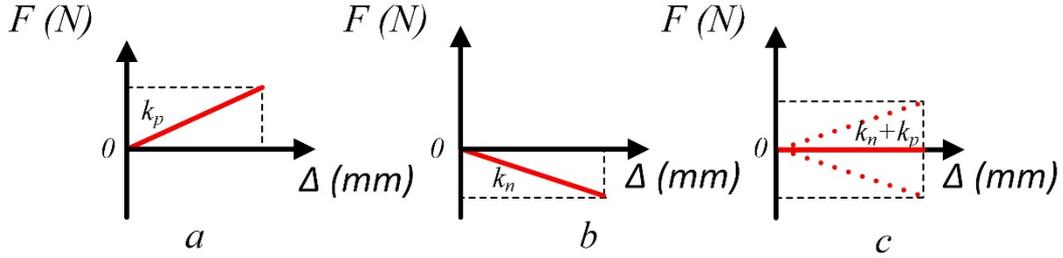

Figure 1. Schematic of the energy balancing system force curve. k_p is the stiffness of the load system and k_n is the negative stiffness system. (a) Increasing force system. (b) Decreasing force system. (c) Energy balancing system.

Although negative stiffness is unusual in engineering systems, appropriate design can be employed to produce the negative stiffness property. The most common negative stiffness structure consists of buckled classic hinged springs with a side pre-load, as shown in Fig. 2 [4], where the springs are under compression in the central position. This creates a local maximum for potential energy, so therefore the central position is unstable while the other two positions are stable. An external load F is applied to actuate the mechanism from one stable position to the other. If the hinged spring is not constrained, the negative stiffness property can cause a sudden snap-through.
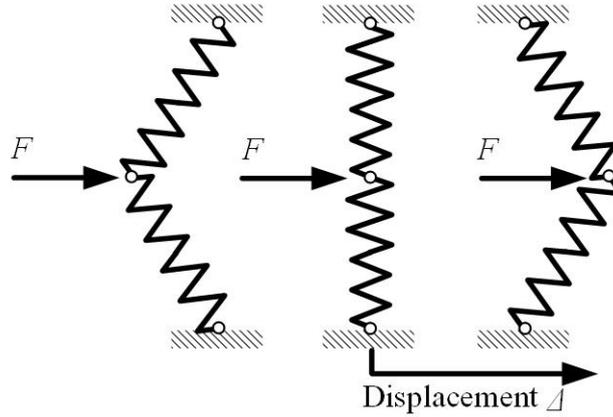
Figure 2. Buckled Classic hinged springs to demonstrate negative stiffness.

Such buckled structures have been employed on numerous mechanical systems where the negative stiffness behaviour can contribute to the required system behaviour. Many applications of the combined system have been investigated, from large-scale honeycomb materials to MEMs-scale switches, including negative stiffness honeycomb materials [5], statically balanced compliant mechanisms [6], negative stiffness–based load-bearing vibration isolators [7], enhanced bimorph strip actuators [8] and highly efficient bridge-type microscale displacement amplifiers [9]. For example, a simple linkage mechanism with a pre-compressed spring linked slider was studied as a negative stiffness device, which could produce passive torque [10]. An analogous springs based system produces a similar effect through a special interaction between a roller and a triangle ramp [11]. A tailored geometry can also generate a negative stiffness behaviour; an optimised spiral pulley was proposed to convert decreasing force into increasing torque output producing a torsional spring with negative stiffness [12]. Some other negative stiffness systems have been produced using non-mechanical phenomena, such as electrostatic forces [13] and magnets [14]. Moreover, a positive and negative stiffness structure can be placed in series to obtain a zero compliance and hence an infinite stiffness [15].

This negative stiffness mechanism can be coupled to the target positive stiffness system to produce an energy balancing system and the energy required to actuate the existing system can be balanced by the stored energy in the negative stiffness system. Figure 3 shows that a net zero stiffness device may be achieved by adding the negative stiffness system to a positive stiffness system, and the coupled system can therefore be considered as an energy balancing system. Fig. 3(a) shows that a traditional way to actuate a system with internal stiffness k_p and the external load L, which required a high power actuator. However, by coupling the negative stiffness mechanism, the total stiffness of the whole system becomes $k_p + k_n$ and is a key benefit is that a lower power actuator can be used to determine the same output with regards to the same external load L, as shown in Fig. 3(b).
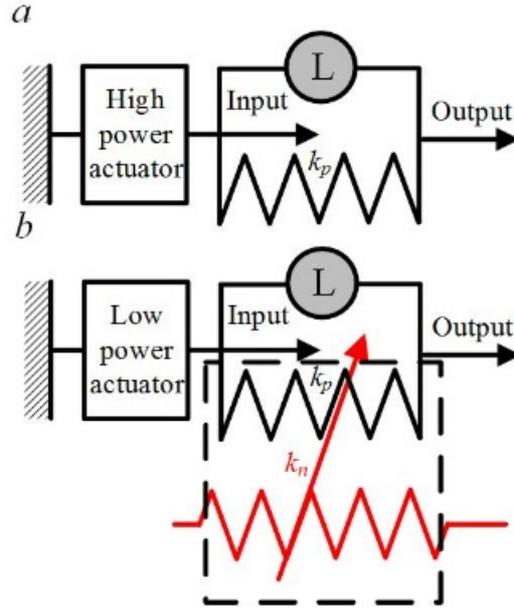
Figure 3. Minimalistic model of a negative stiffness mechanism for energy balancing. L denotes the external load, k_p is the internal stiffness of the load system and k_n is the negative stiffness system. (a) Traditional actuated system. (b) Energy balancing system by adding the negative stiffness mechanism.

It can be assumed that if the required input, such as force or torque, can be completely eliminated by the negative stiffness system, then in principle no energy is required to move the system, other than to overcome dissipation. Therefore, the use of negative stiffness systems is likely to benefit energy constrained systems, such as those present in the aerospace and automotive industries. Many applications have been proposed that use a negative stiffness for passive energy balancing. An adjustable constant force mechanism has been proposed, which consists of a linear positive stiffness mechanism and a linear negative stiffness mechanism. The linear negative stiffness mechanism is obtained by using a cam mechanism, where the cam profile has been designed to generate a constant force output [16]. Similarly, a cosmetic glove stiffness compensation mechanism has been designed by using a negative stiffness element. This negative stiffness element is designed as a rolling stiffness compensation mechanism by using linear helical springs as energy storage and a rolling link mechanism. By using a negative stiffness element, a smaller size mechanism can be built and the maximum operation forces are reduced with satisfactory efficiency [17]. A statically balanced compliant mechanism has been proposed by coupling a compliant mechanism with a pre-compressed plate spring, to give a zero-stiffness behaviour [18]. Some other alternative uses of negative stiffness systems for passive energy balancing have also been investigated, such as for morphing aircraft. A negative stiffness nonlinear over-centre linkage is used on a tilt-rotor blade for active twist. This negative stiffness linkage mechanism uses the stored energy of a compressed spring to rotate the output shaft, resulting in an effectively softened blade that requires 70% reduction in torque for morphing [10]. In addition, a pulley based balancer has been proposed with a varying radius pulley to preserve moment equilibrium between a constant load and a varying spring length. By using such a spiral pulley negative stiffness mechanism, the required torque for the morphing actuation can be satisfactorily matched to create a nearly zero stiffness which required minimal energy [12]. The proposed device provides actuation to change the state of the system, such as deforming a structure or lifting a mass; hence the energy provided by the actuator transforms into an increased potential energy in the system. Once the system returns to its original state, all of the energy provided by the actuator will be recovered, if the system is conservative. In other words, the work done to reach the target state require the input of energy, while the subsequent dissipation of that energy to recover the initial state generates waste heat.

Although negative stiffness devices have been proposed previously, an innovative concept for designing an integrated Bidirectional Torsional Negative Stiffness (BTNS) mechanism is presented in

this paper. Many current negative stiffness devices were designed for static force balancing, which is unidirectional. For example, a spiral-shaped pulley has been used to create negative output stiffness by converting decreasing forces in a prestretched extension spring into increasing torque output[12,19]. Such spooling pulley systems will be limited by the warp direction and can only provide one-way actuation, which is fundamentally limited to unidirectional response due to the requirement for the drive spring to remain in tension. Moreover, most mechanisms designed as negative stiffness for static gravity equilibrators use prestressed components, such as prestressed torsion bars [20], and the motion of the mechanism should be opposite to the prestress direction. The discussed negative stiffness mechanisms [12,19,20] are unidirectional and this limitation restricts further applications. Figure 4 shows a schematic of the integrated system force curve by coupling two kinds of negative stiffness system. Many energy required systems have a bidirectional elastic force response as shown in Fig. 4(a). As we discussed, the negative stiffness can be used to produce static balancing for such systems with a zero stiffness property, which can be seen in Fig. 4(b) and 4(c). However, a bidirectional negative stiffness system is possible to provide an energy balancing system where the actuation is zero, as shown in Fig. 4(b). The unidirectional negative stiffness system can only release the force/torque in one direction to produce a zero stiffness integrated system, which still requires energy for actuation. Therefore, the bidirectional negative stiffness should be investigated for passive energy balancing of mechanical systems to reduce actuation requirements and improve energy efficiency.
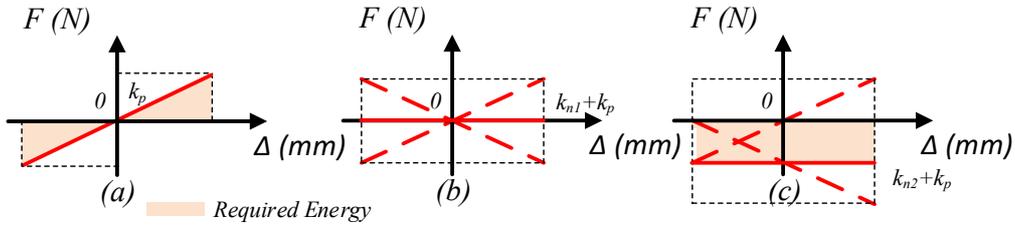

Figure 4. Schematic of the integrated bidirectional system force curve. k_p is the stiffness of the load system and k_{n1}, k_{n2} are the negative stiffness systems. (a) Bidirectional increasing force system. (b) Integrated system of (a) and a Bidirectional negative stiffness system. (c) Integrated system of (a) and a unidirectional negative stiffness system.

Some structures were devised by using a bi-stable structure to exhibit bidirectional negative stiffness. Because it is difficult to achieve a negative stiffness in two directions, a combination of bi-stable mechanisms can be easily performed. A bidirectional negative stiffness structure utilising buckling phenomena has been investigated with regard to new broadband metamaterials [21], which provides a linear motion for the driven system. However, this research focuses on a new negative stiffness mechanism, the bidirectional torsional negative stiffness (BTNS) mechanism, that is capable of generating the satisfactory torque versus rotation profile and overcome some drawbacks of current negative stiffness devices based on pulley concepts such as [12]. The energy used in an actuator is usually non-recoverable, but the BTNS device can provide energy to actuate and then be back-driveable by the elastic load in the system. It is important to note that the combination of a negative stiffness and a positive stiffness is likely to build a system that can recycle energy; for a conservative system this recycling will be perfectly efficient. Thus the BTNS device can help to compensate for the required force/torque and energy and therefore use a smaller (and lighter) actuator. Therefore, this BTNS mechanism can be more beneficial than fixed directional negative stiffness devices In addition, based on a modularized design, the BTNS device can be integrated to provide substantial force/torque, and so it may be applied to different application areas of passive energy balancing. The reconfigurability of the device allows it to be easily customised for different conditions, for example, several smaller (BTNS) units could be used in place of a single larger unit to satisfy any given space limitations.

This paper proceeds as follows. Firstly, the structure of the device is illustrated using a LEGO® prototype. The kinematics of the bidirectional torque shaft and rotation angle are investigated, and the

proposed LEGO® prototype is tested to verify the precision of the analysis. Then, a prototype of this BTNS device is fabricated and the corresponding torque is compared between the experimental and analytical results. Moreover, a potential application of morphing the camber of a wing is illustrated by coupling the BTNS device and the predicted torque, required energy and evolution of efficiency are shown numerically. Finally, the design parameters is optimised to exactly match the requirements of the morphing actuation.

2. BTNS concept and method

The BTNS mechanism is constructed from a series of pre-compressed springs that store the energy, coupled with a shaft to convert axial motion and force into rotary motion and torque. The geometrical parameters can be chosen to generate a wide range of output torque versus rotation.

In order to demonstrate the BTNS concept, a physical model was made from LEGO® and is shown in Fig. 5. LEGO® bricks have been widely used, especially for demonstration purposes, in a variety of scientific fields, including mechanisms [22,23], biological sciences [24], and physics [25,26]. In this research, bricks of selected size and shape can be placed at designated locations to reproduce the negative stiffness behaviour of the constructed mechanism. The device is presented here as a 2D structure, however an example of how it may be incorporated into a 3D wing structure will be shown later.
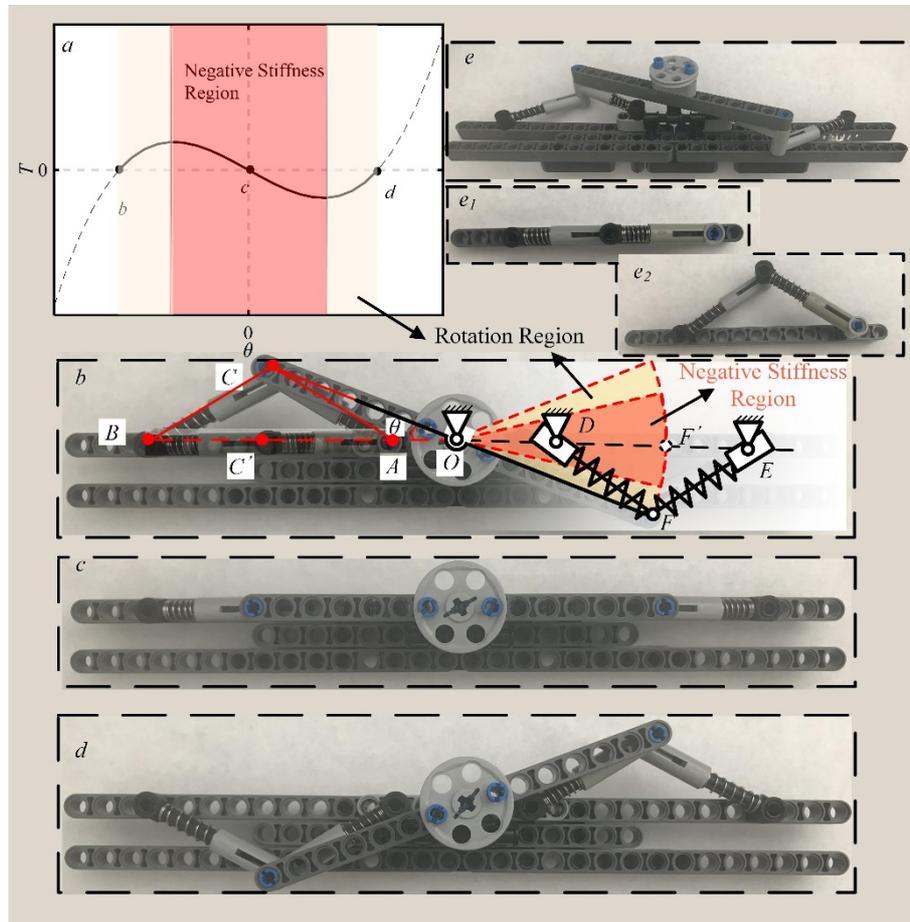

Figure 5. A LEGO® realization of a BTNS mechanism. (a) Torque- rotation characteristic diagram and a localised negative stiffness is shown. Points b, c and d represent the states shown in Figs (b), (c) and (d), respectively. (b) A kinematic view of the BTNS prototype with schematic geometry analysis. (c) A view of the BTNS prototype in the initial state. (d) A view of the BTNS prototype in the other direction state. (e) Isometric view of the BTNS prototype. (e_1) A view of the spring mechanism at its maximum energy position. (e_2) A view of the spring mechanism at its minimum energy position.

The energy-storage element is constructed using LEGO® springs, which are compressed in the horizontal direction. The mechanism effectively has a single degree of freedom system, which is the

rotation of the central shaft. Two equilibrium positions of the energy-storage element, namely an unstable equilibrium (maximum energy) and one of the stable equilibria (minimum energy), are shown in Figs. 5(e$_1$) and 5(e$_2$) respectively. After these energy-storage elements are installed in the BTNS prototype shown in Fig. 5 (e), the central pulley rotates on the out-of-plane axis, causing the energy-storage element to be released to produce torque. Figure 5a shows a typical torque rotation characteristic for the BTNS prototype, showing that the negative stiffness properties of the spring mechanisms result in a region of negative torsional stiffness in the overall device. Figure 5(c) shows the zero rotation angle of this BTNS prototype in the initial position C' and mark points c in Fig 5(a). The associated schematic geometry analysis of this BTNS prototype is shown in Fig. 5(b), which plots the detailed configuration after clockwise rotation to marked points b in Fig 5(a). Figure 5(d) plots the configuration after anticlockwise rotation to marked points d in Fig 5(a).

Moreover, the concept can be illustrated from the viewpoint of kinematic analysis. The rigid link OF is fixed with an output pulley as shown in Fig. 5(e); the torque will be transmitted by this pulley to the driven structure. Initially, the BTNS prototype will be situated in the zero rotation angle position as shown in Figure 5(c), which means the links OF, EF and DF are oriented in the horizontal direction (i.e. joint F is located at F'), and the springs are at maximal compression. Then, because this position is a maximum energy point, rotation about this point will exhibit a region of negative stiffness, driven by the compressive forces in the springs. Therefore, the link OF is driven and the pulley can finally be actuated to rotate clockwise or anticlockwise. The BTNS prototype is assembled by a series of rigid elements and elastic elements to transfer force to torque, and based on the energy-storage elements such output torque presents a negative stiffness in a certain range. In order to investigate relationship between the negative stiffness property and the motion range, a more detailed kinematic analysis will be presented in Section. 3.

3. Bidirectional torsional shaft analysis

The detailed geometry definition of one element is shown in Fig. 6. The shaft is centred at O and θ is the shaft rotation angle. In order to determine the length of the moment arms and the amount of drive spring displacement, the kinematics can be derived as follows.
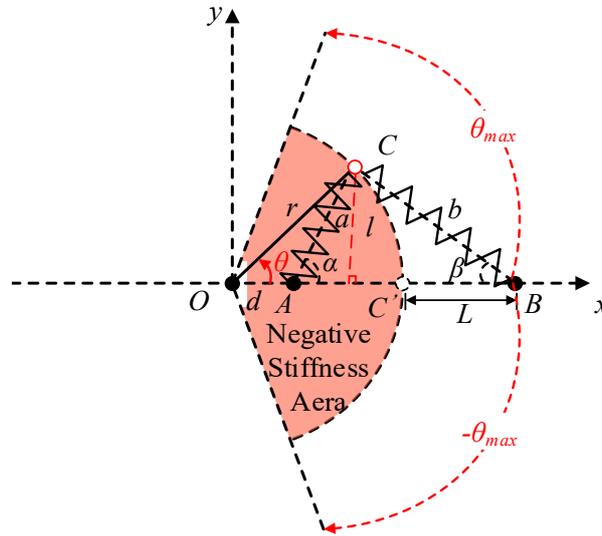

Figure 6. Geometry analysis of BTNS mechanism with moment arm details. Point O is the rotation centre, lines AC and BC are the compressed springs and points C and C' represent the operated position and the initial position, respectively.

The two springs are represented by lines AC and BC and the position of point C is given by:

$$x_C = r \cos \theta \tag{1}$$

7

$$y_C = r \sin \theta \qquad (2)$$

where r is the radius of the torque shaft. The length of the spring $\overline{AC}$ is equal to

$$a = \sqrt{(x_C - d)^2 + y_C^2} = \sqrt{(r \cos \theta - d)^2 + (r \sin \theta)^2} \qquad (3)$$

Then, point C' is the midpoint between A and B, and the initial position of point C. The length of the vector $\overline{AC'}$ and $\overline{C'B}$ is defined as L. The length b of the vector $\overline{BC}$ can be obtained from the known d, r and L, as

$$b = \sqrt{\left(2L - (x_C - d)\right)^2 + y_C^2} = \sqrt{\left(2L - (r \cos \theta - d)\right)^2 + (r \sin \theta)^2} \qquad (4)$$

Moreover, the length l of the perpendicular line is equal to y_C

$$l = y_C = r \sin \theta \qquad (5)$$

With a, b and l now known, the law of cosines can be applied to find the angles α and β as

$$\alpha = \sin^{-1}\left[\frac{l}{a}\right] = \sin^{-1}\left[\frac{r \sin \theta}{\sqrt{(r \cos \theta - d)^2 + (r \sin \theta)^2}}\right] \qquad (6)$$

and

$$\beta = \sin^{-1}\left[\frac{l}{b}\right] = \sin^{-1}\left[\frac{r \sin \theta}{\sqrt{\left(2L - (r \cos \theta - d)\right)^2 + (r \sin \theta)^2}}\right] \qquad (7)$$
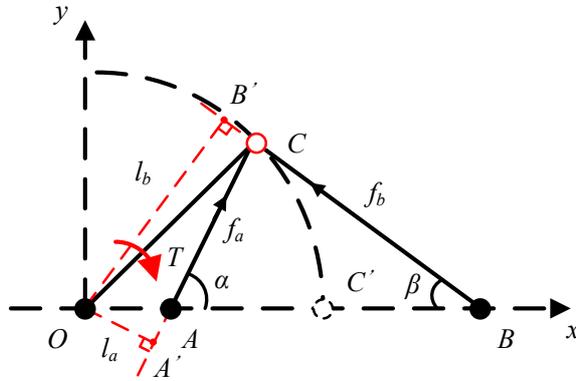

Figure 7. Mechanics of the BTNS mechanism.

Since the torque shaft is connected to the compressed springs at point C, as shown in Figs. 6 and 7, the rotation of the torque shaft leads to the release of a portion of the compressed springs. The change of the spring force can be calculated by subtracting the length L_θ evaluated at the current shaft rotation angle θ, from the length L_0 at the initial shaft rotation angle θ_0, which for this analysis is 0.

$$\Delta L = |L_\theta - L_0| \qquad (8)$$

The drive spring is designed as an energy storage device with an initial length L_0 as mentioned above; the force in the drive spring at current position, f, can therefore be obtained as

$$f = K\Delta L \qquad (9)$$

8

where K is the drive spring constant. Therefore, the force provided by the two springs can be obtained as

$$f_a = K_a(a - L_0) \tag{10}$$

and

$$f_b = K_b(b - L_0) \tag{11}$$

In addition, the moment arm at which the force in the spring acts is defined by the vector that passes through point O, that is, l_a for the moment arm $\overline{OA'}$ and l_b for the moment arm $\overline{OB'}$. These two moment arms can now be obtained as

$$l_a = d \sin \alpha \tag{12}$$

$$l_b = (d + 2L) \sin \beta \tag{13}$$

Finally, the total torque resulting on the shaft from the drive springs acting at its current rotation angle θ will be obtained from Eq. (10) - Eq. (13) as

$$T_o = f_a l_a + f_b l_b \tag{14}$$

The evolution of the drive torque as the shaft rotates is the key to this analysis, and the equations above provide a detailed description of the force-displacement response of the BTNS mechanism. This introduces the geometry of this mechanism and can provide the best performance for a given design case.

Moreover, the angular range over which the BTNS mechanism shows negative stiffness is required to understand its suitability for a given application. Figure 5(a) shows the torque-rotation characteristic diagram of a BTNS mechanism, and the negative stiffness region is terminated when the maximum torque occurs. So the maximum operating range of the BTNS mechanism can be estimated by considering the slope of the torque-rotation curve and given by

$$\frac{dT_o}{d\theta}|\theta_{max} = 0 \tag{15}$$

Then, in order to validate the accuracy of the prediction from the analysis, the LEGO® model proposed in Section 2 is tested here. The experimentally measured torque is now considered and compared with the predictions from the analysis. The stiffness of the spring will be used in the analytically predicted evolution of torque for the LEGO® model with a measured stiffness of $K = 570.1$ N/m. The constant radius r of the torque shaft was fixed at 57 mm.

Figure 8 shows the experimentally measured and analytically predicted evolution of torque for the LEGO® model. For the analysis, the torque is calculated until the maximum absolute value is reached. Since the mechanism is a symmetric system, only one direction test is measured and the opposite direction is assumed to have the same curve. The test rig was mounted on a material test machine for displacement cycling, and both the torque and rotation angle can be calculated from the data from the material test machine. It can be seen that the initial linear portion of the torque can be captured properly and a minor offset of the torque occurs in the nonlinear portion. This is the result of friction in the system and the flexibility of the LEGO® bricks. This physical model shows a satisfactory prediction of the general behaviour of the BTNS mechanism. If the required torque for morphing the target practical structure was from 0 to 0.5 Nm, this LEGO® BTNS mechanism can even be used for actuation. The possible range of the motion is 18 degrees, but when the motion exceeds 10 degrees the device will exhibit positive stiffness as illustrated in Fig. 5(a).
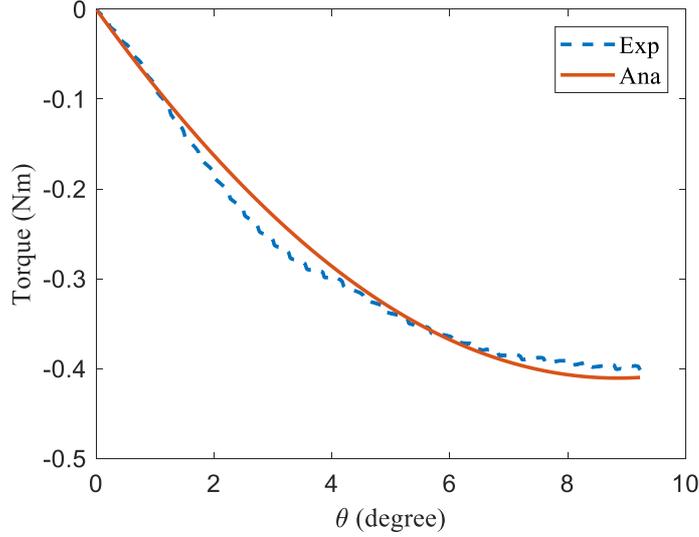
Figure 8. Comparison of the experimental (Exp) and analytical (Ana) torques for the LEGO® BTNS mechanism.

4. Design case

In order to show the broad scope of applications envisioned for this BTNS mechanism, a generic design case will be proposed here. The system is intrinsically scalable, limited mainly by the required components, such as drive springs, bearings, and cordage of different sizes. The test demonstrator was built to allow for experimental testing and validation of the BTNS concept and the proposed analysis. This test device was generated by using computer-aided design as shown in Fig. 9 and constructed by various components. Figure 9 shows a full scheme of the integrated BTNS system and a schematic diagram of the proposed BTNS unit. The BTNS units are connected by the rotation shaft so that each unit can provide an effective torque for the load system. It is worth mentioning that the BTNS unit can provide a bidirectional motion by rotating the shaft clockwise (B) or anticlockwise (A), as shown in Fig. 9. This bidirectional feature provides a better solution for many practical applications than single directional devices. The dimensions and the corresponding parameters of the BTNS unit are carefully selected based on the previous LEGO® model.

Table 1. BTNS mechanism parameters for energy balancing test.

Parameter	Value	Units
Drive spring rate, K_a	1.8	N/mm
Initial spring length, L_0	33	mm
Mounting distance from origin, d	10	mm
Mounting distance, $2L$	52.6	mm
Output pulley radius, r_p	10	mm
Bidirectional shaft radius, r	36.3	mm

Table 1 shows the key parameters of the BTNS unit and only four springs are used. All the components used here are ubiquitous and already manufactured over a very broad range of scales. The intention of this initial study is therefore to show the considerable energy storage achievable in a moderate size demonstrator.
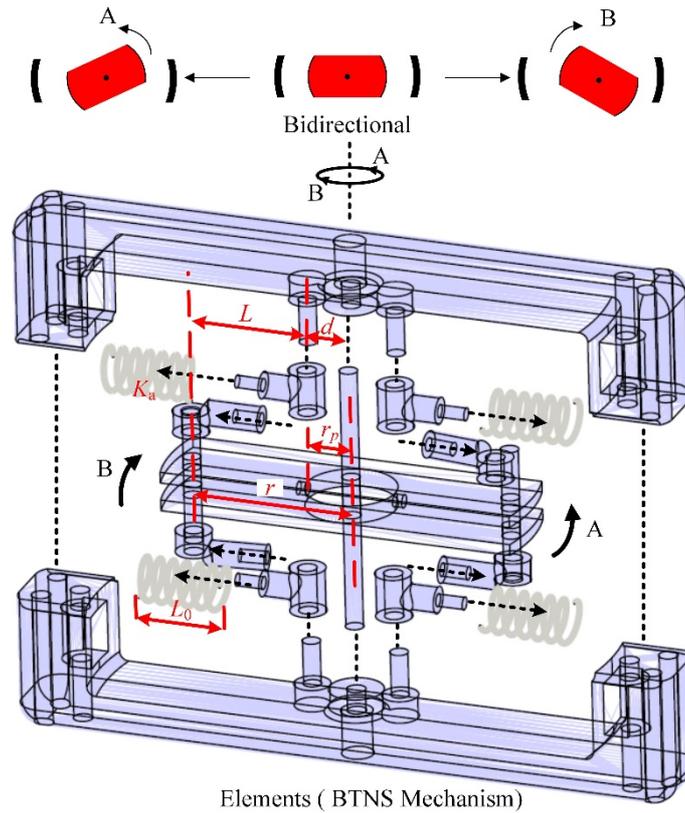
10

Figure 9. Schematic diagram of the proposed BTNS mechanisms with the indicated parameters in Table 1.

A side view of the completed test device is shown in Fig. 10(a). The pulley was mounted onto a central shaft which was supported by radial bearings mounted to the frame, as shown clearly in Fig. 10(a). High-strength spectra cordage was wrapped around the constant radius pulley and may be connected to the load system for actuation. The pulley and frame components of the device were three-dimensional (3D) printed from photosensitive resin on a fused deposition modelling printer (UnionTech 3D Printer). All of the four springs are compressed and the arrangement of the additional components allows the springs to store the potential energy.

Once assembled, a material test machine (Zwick/Roell) is used to obtain the force displacement curve. As seen in Fig. 10(b), the BTNS device was mounted to the moving grips of the test machine. The device was aligned such that force could be applied directly to the cordage attached to the upper crosshead of the testing machine. The corresponding torque required was calculated by multiplying the directly measured force by the known radius of the pulley. The angle of the rotation of this spinning pulley shaft was obtained by dividing the measured displacement by the known radius of the pulley. A 2.5 kN load cell was installed between the cordage and the crosshead to record the tension applied to the device.
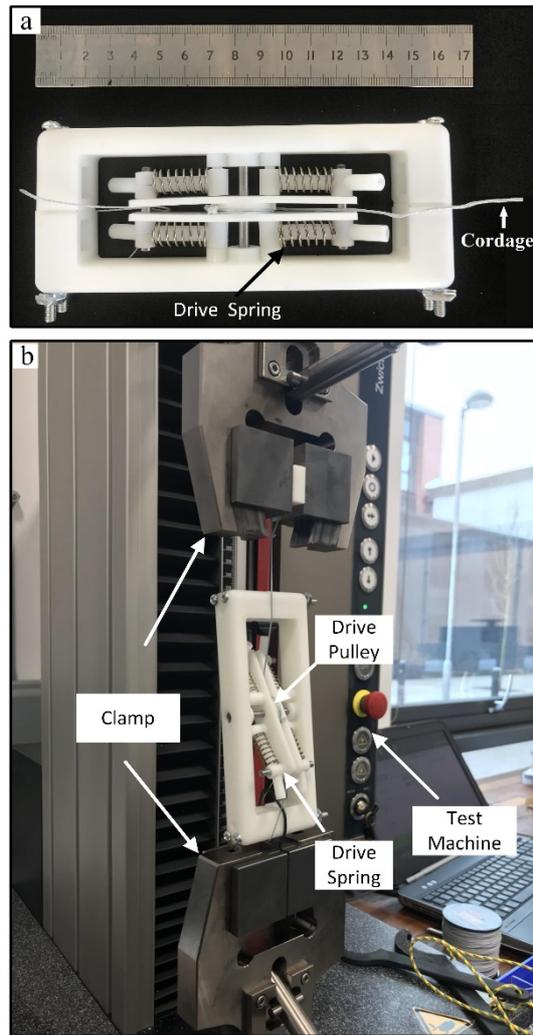
Figure 10. A 3D printed BTNS mechanism. (a) Side view of test rig showing pulley mount. (b) BTNS mechanism test rig.

The experimentally measured torque is now compared to the predictions from equations (10) to (14). The constant radius r_p of the torque pulley was 10 mm, which was wrapped by a high-strength spectra cordage. Figure 11 shows the experimentally measured and analytically predicted evolution of the torque for the BTNS device. The maximum operating range of this case is 31 degrees as shown in Fig 11, which can be also estimated by equation (15). These torque results show that the experimental curve is not smooth and a minor offset of the torque exists between the experimental result and the analytical prediction. This is the result of the assembly method used and friction in the system. As shown in Fig. 9, the springs were compressed and then applied via a sleeve onto the rotatable axle and the rotatable axle was assembled with the frame. For this reason, once the device rotated, a jump in the spring length can occur which will cause the non-smooth force profile. However, in the further development of the BTNS device, the friction will be reduced by using suitable bearings and a positioner can be used to restrict the compressed spring. In general, this physical model shows a satisfactory prediction of the general behaviour of the BTNS device.
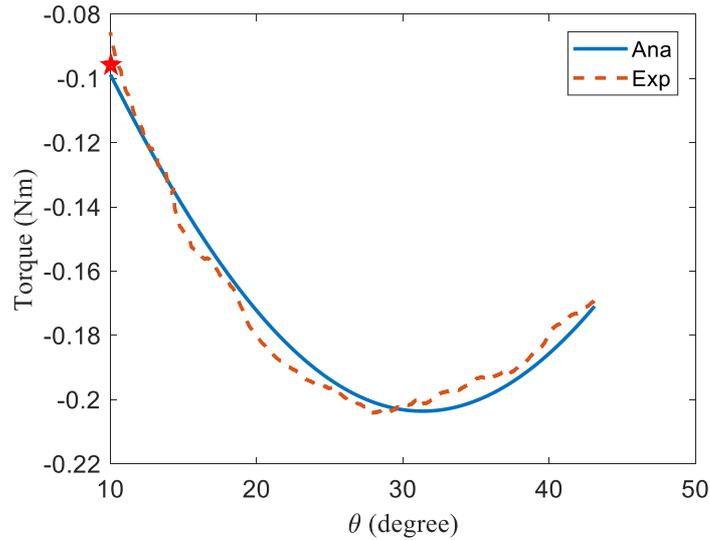
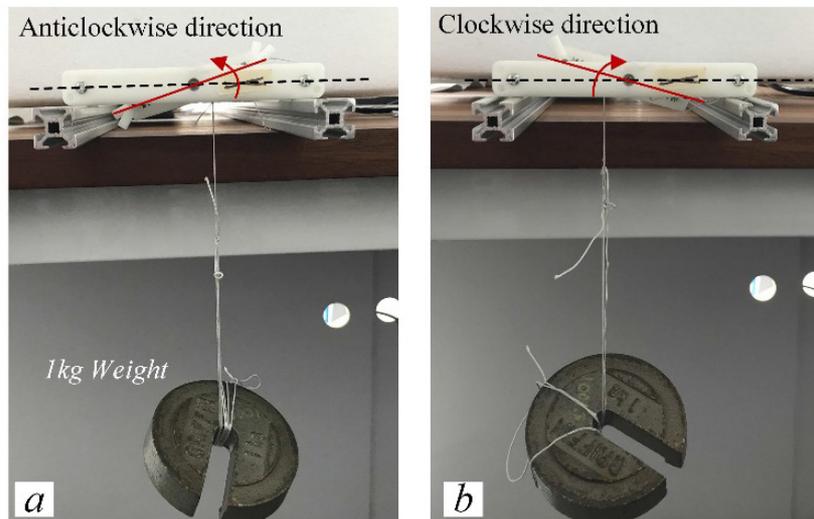**Figure 11.** Comparison of the experimental and analytical torque.

Figure 12. Bidirectional static balancing experiment.

In order to illustrate the bidirectional property of the BTNS mechanism clearly, a bidirectional static balancing experiment is shown. A 1 kg weight is hung to give an anticlockwise and clockwise moment on the output pulley where the moment arm is given by the pulley radius, r_p. The pulley rotation angle θ is 10 degrees, which is measured by a contactless angle sensor (Gill Sensors Part #1498-00-068) directly. The corresponding result is shown in Fig. 11 and marked as a star. While this experiment is simple, it provides experimental verification of the bidirectional stiffness.

Having established the basic operating principle and experimental validation of the BTNS mechanism, the case of a morphing aircraft wing section will illustrate the performance of the BTNS concept.

5. Case study: morphing wing section and optimisation
After showing the experimental validation of the predicted results, the integrated BTNS mechanism and the possibility to passively balance the energy requirements of a practical engineering application will be discussed. In order to show the efficacy of the passive energy balancing concept by using the BTNS mechanism, it is useful to consider a representative design scenario. The initial study here will show how the BTNS mechanism can be applied for energy balancing in a morphing application, as most morphing applications require external actuation, and many have high internal structural loads to overcome, for example [27]. A recently introduced active camber concept known as the fish bone active camber (FishBAC) mechanism is considered as the load in this paper [28,29]. In this case, both

the aerodynamic load and the elastic deformation of the structure were considered and the analytical formulation was derived from Euler-Bernoulli beam theory. While this BTNS mechanism cannot replace the actuator since an actuator is always needed to set and maintain the desired position, it could decrease the maximum force required and decrease the work supplied by the actuator, resulting in a lighter actuator. Figure 13 shows a schematic of the proposed BTNS mechanism for a potential application of bidirectional morphing aircraft actuation. The FishBAC is driven by a tendon and acts as the target positive stiffness system; the torque shaft of the BTNS device is installed as part of the tendon spooling pulley. A circular array of compressed springs is constructed to give a negative stiffness unit and then assembled as an integrated BTNS mechanism located in the wing spar.
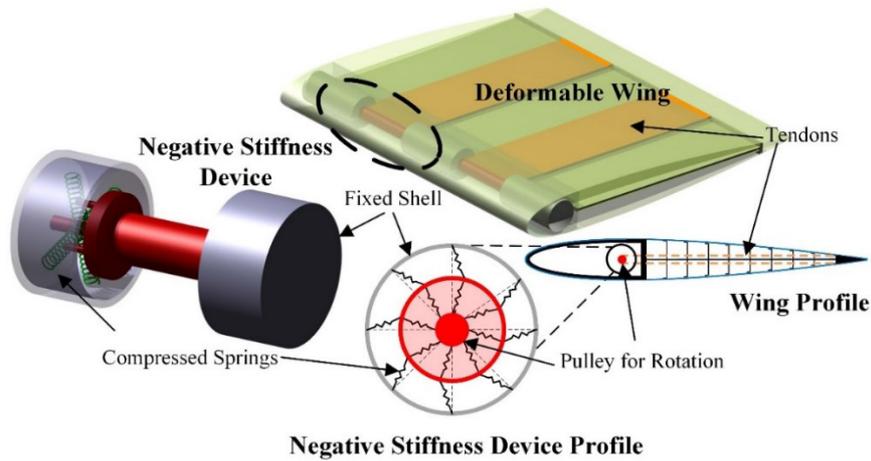

Figure 13. Schematic of an integrated BTNS mechanism for morphing aircraft actuation.

Figure 14 shows the predicted shapes of the morphed profiles for the range of the tendon pulley rotation angles studied, along with a schematic representation of the spine bending displacement. This structural model is analytical and derived from Euler-Bernoulli beam theory, and the torque produced by the pulley rotation is assumed to induce a moment on the FishBAC [28].
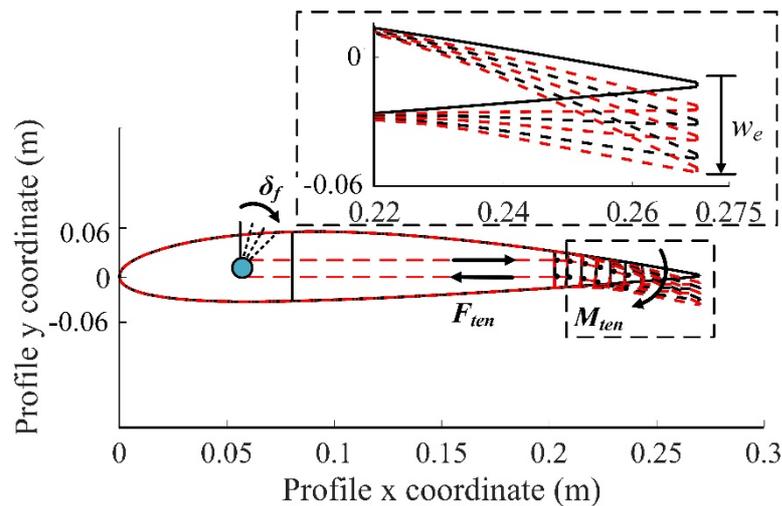

Figure 14. Deflection of the objective morphing aircraft model.

The required moment to actuate the active camber is provided by a rotary actuator, which can be solved by prescribing the tendon spooling pulley rotation angle, as shown in Fig. 14. The relationship between the pulley rotation and the required moment is shown in Fig. 15. This active camber concept can be considered as a general positive stiffness system as the required moment is directly proportional to the rotation angle. Therefore, the required torque for morphing will give the target positive stiffness system for designing the BTNS mechanism in the following research. A negative

14

stiffness system will be investigated here as a means to transfer the energy required for different morphing configurations of the active camber.
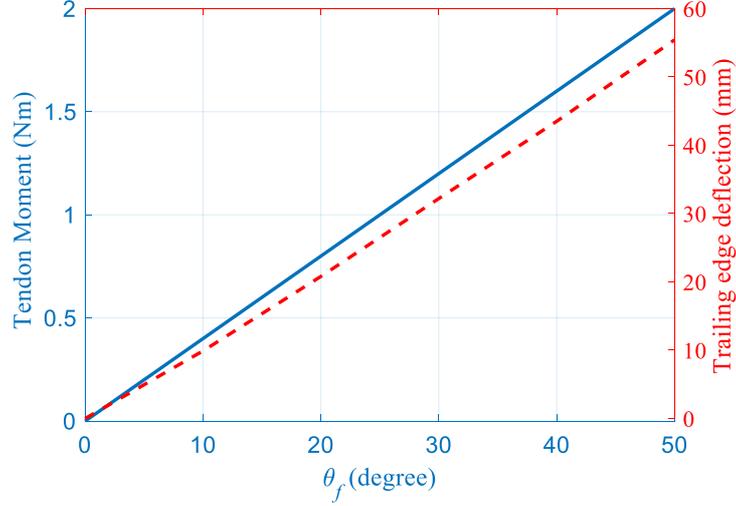

Figure 15. Actuation moments (solid line) and trailing edge deflection (dashed line) versus spooling pulley rotation.

Furthermore, one impact of such a BTNS mechanism is that the performance will be restricted by the fixed geometry, such as the maximum rotation angle. This will require the use of a mechanical element to transmit different torque and rotation. To accomplish this, a gear is proposed here, which has the ability to modify the gear ratio G between the actuator output and the target morphing structure. This allows the torque to be optimised for the required combination of output torque and rotation angle. When these two independent systems are connected by a gear, the resulting torque T_f on the FishBAC tendon spooling pulley will be modified by the gear ratio G to give

$$T_f = T_o G = (f_a l_a + f_b l_b)G \tag{16}$$

The corresponding rotation of the load system is also be modified as

$$\theta_f = \frac{\theta}{G} \tag{17}$$

The BTNS unit shown in Section 4 is first used here as a general way to fit the device into the morphing wing and the existing parameters are shown Table 1. In addition, two other parameters are considered here, which are the gear ratio $G = 0.5$ and the number of BTNS units (here we assume $n = 10$). The performance predicted by equations (10) to (14) for the energy balancing system shows satisfactory matching of the torque requirements of the FishBAC mechanism well. The evolution of torque with rotation for the negative stiffness system, the positive stiffness system and the net torque of the whole system is shown in Fig.16. The torque provided by the integrated mechanisms constructed by ten BTNS units matches the torque required closely, and the maximum torque required by the actuator is less than 0.2 Nm. In other word, the morphing system with the BTNS device only requires a small actuator for stabilising the coupled system.

It should be noted that the net stiffness of the system shown in Fig. 16 shows regions of negative stiffness, and this must be avoided if it is to remain stable. However, this graph only shows the contribution of the structure and negative stiffness device, and neglects any additional stiffness added through the presence of the actuator, which will sufficient to restore stability if the negative stiffness is small. However, if the actuator stiffness is insufficient, the negative stiffness must be reduced to maintain positive stability.
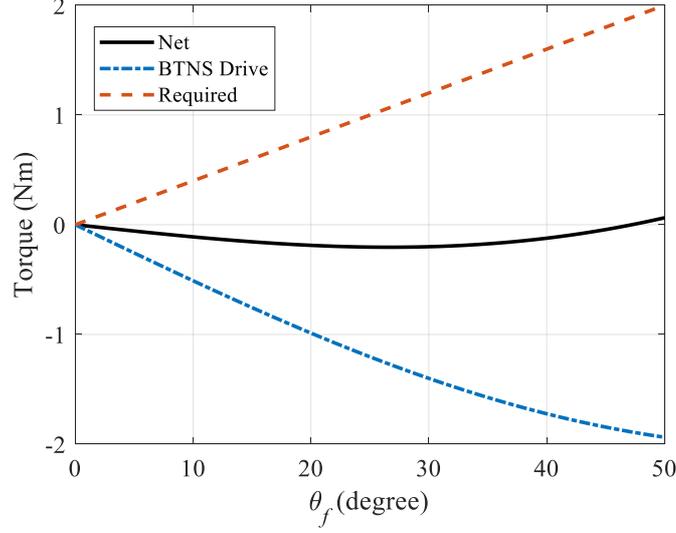
Figure 16. Predicted torque with the BTNS mechanisms.

Moreover, in order to evaluate the performance of the energy balancing system, it is useful to establish an efficiency metric. First, the energy available E_o is the maximum amount of the energy that the BTNS mechanism could theoretically produce from a zero angle to the current position. This can be written as

$$E_o = \int_0^\theta |T_o| \, d\theta \tag{18}$$

Second, the energy required E_r is simply the energy associated with moving the load. This will be the integral of the required torque with respect to the angle and is equal to

$$E_r = \int_0^{\theta_f} |T_f| \, d\theta_f \tag{19}$$

Finally, the net input energy E_n required by the actuation will be the total amount of energy put into the system from the zero angle to the current angle θ and is equal to

$$E_n = |E_o - E_r| \tag{20}$$

For this rotary system, an energy conversion efficiency metric η_{ef} can be defined as

$$\eta_{ef} = 1 - \frac{E_n}{E_r} \tag{21}$$

This is a meaningful metric to evaluate energy between these two systems: the negative stiffness system and the positive stiffness system, as this implies the energy transfer efficiency during actuation. With this energy conversion efficiency metric, an equivalent energy comparison can also be potentially used to provide a better match of the required torque for the BTNS mechanism. Figure 17 shows the mechanical energy required to morph the target active camber, which is provided by integrating the torque (T_o and T_f) versus rotation angle. By comparing the energy required with and without the BTNS mechanism, it shows that the BTNS mechanism has a strong ability to passively balance the required torque.
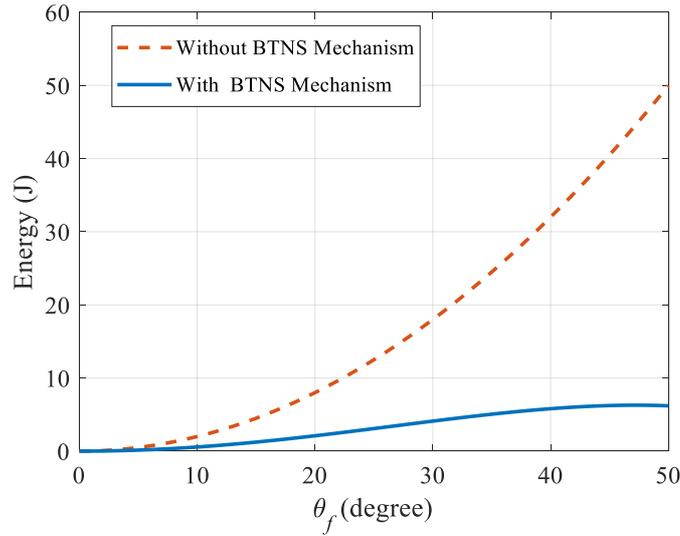
16

Figure 17. Comparison of predicted energy required with and without the BTNS mechanisms.

A further view of the effective reduction of the actuation energy requirements during the operation can be seen in Fig 18. The energy conversion efficiency metric η_{ef} is plotted against the rotation angle θ_f, and it is seen that the efficiency is greater at higher angles. Figure 17 shows that the maximum predicted energy reduction is almost 90%, with the energy required reduced from 50 J to 6 J. This is the contribution of the energy that is stored in the BTNS units in the initial position.
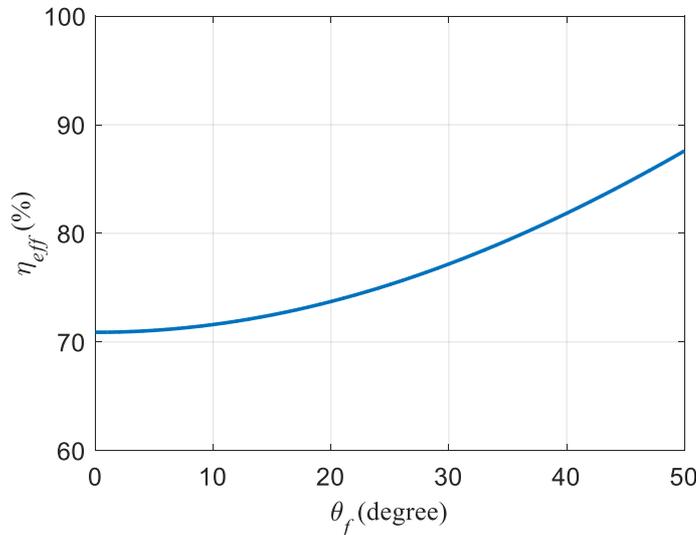

Figure 18. Evolution of efficiency with rotation angle of the energy balancing system.

However, the proposed BTNS mechanism cannot exactly match the required torque profile in this case as the parameters are not optimised for this aircraft actuation case. Therefore, a more practical way is presented to apply such BTNS mechanism as an example to show that each component of the mechanism can be used to improve performance corresponding to the target application. Therefore, in order to maximise the performance of the energy balancing system, the geometric parameters of the BTNS device are optimized using the *fmincon* function in Matlab. The energy conversion efficiency metric η_{ef} is used as the objective function to make the torque available from the BTNS mechanism match as closely as possible the requirement for morphing the aircraft over the entire prescribed

rotation range. The upper and lower bounds set for the optimisation design are given in Table 2. These bounds are practical and realistic restrictions on the design space.

Table 2. Design parameters for the BTNS optimisation.

Parameter	Lower bound	Upper bound	Optimised value	Units
Drive spring rate, K_a	0.1	3.5	2.40	N/mm
Drive spring rate, K_b	0.1	3.5	1.80	N/mm
Initial spring length, L_{10}	10	50	33.39	mm
Initial spring length, L_{20}	10	50	32.99	mm
Mounting distance from origin, d	5	45	10.54	mm
Mounting distance, $2L$	20	200	105.20	mm
Bidirectional shaft radius, r	15	50	35.89	mm
Gear ratio, G	0.1	1	0.1	-
Numbers of BTNS units	1	20	2	-

The performance predicted for the optimised BTNS mechanism shows a better match to the morphing torque requirements. Figure 19 shows the evolution of torque with rotation for the negative stiffness system, the positive stiffness system and the net torque of the whole system. The torque provided by the integrated mechanisms constructed by two optimised BTNS units matches the torque required perfectly, which reveal that the optimiser is able to find solutions for a lower net torque.
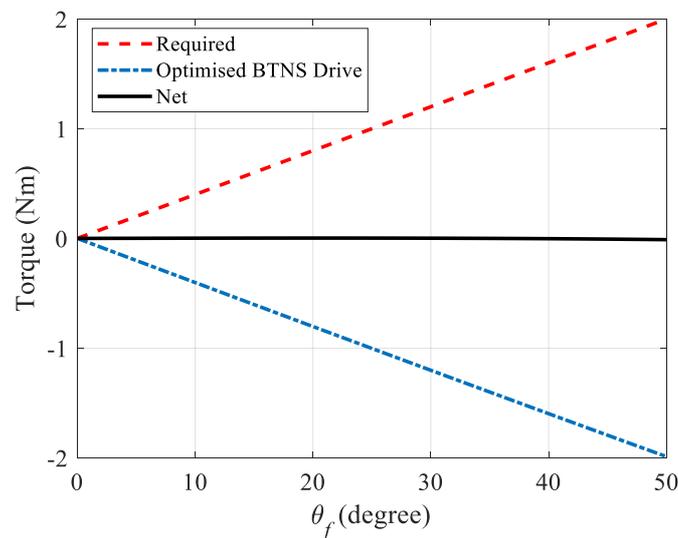

Figure 19. Predicted torque with optimised BTNS mechanisms.

The mechanical energy required for morphing the aircraft can be calculated by integrating the torque versus rotation curves, as shown in Figure 20. By comparing the energy required for the morphing alone to that with the BTNS device and the optimised BTNS device attached, the ability of the negative stiffness device for energy balancing can be seen. The maximum predicted energy reduction is almost 99% with the optimised BTNS device attached. Each optimised BTNS device is therefore predicted to be able to store and passively transfer 25 J.
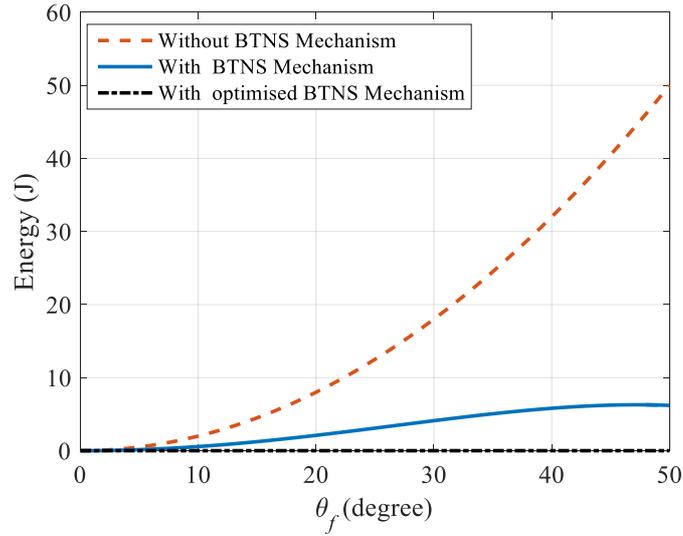
Figure 20. Comparison of predicted energy required with and without optimised BTNS mechanisms.

Figure 21 gives a further view of the effective reduction of the actuation energy requirements during operation, where the energy conversion efficiency metric, η_{ef}, is plotted against the rotation angle, θ_f. Both BTNS devices exhibit increases in efficiency with rotation, but the optimised BTNS device can maintain a higher efficiency over the entire prescribed rotation range.
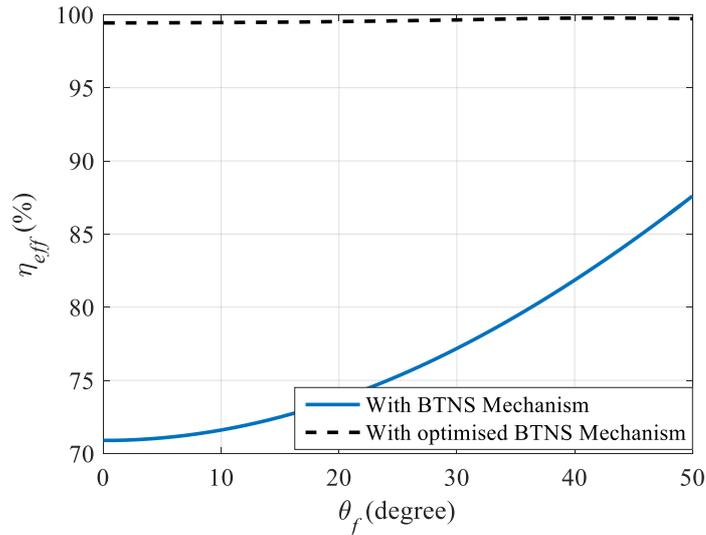

Figure 21. Evolution of efficiency with rotation angle of the energy balancing system with and without optimisation.

Based on this investigation, the integrated BTNS mechanism can provide a significant contribution to balancing the positive stiffness system, such as the proposed FishBAC mechanism. In some practical applications, the external disturbance, such as the aerodynamic load or hysteresis behaviour of a wing, will influence the negative stiffness mechanism to eliminate the required force or moment completely. But high energy conversion efficiency can be optimised; most of the required energy can be balanced by using the BTNS mechanism, and a small actuator could be used to compensate the difference between these two systems. The work presented here is intended to show the energy balancing concept and the tailorability to different positive stiffness systems. Although the improvement provided by the integrated BTNS mechanism is shown for a specific load case, the underlying reason for its effectiveness is present in a wide range of applications, including different actuators and many different load profiles to be driven.

6. Conclusion

A new concept for a BTNS mechanism by using a series of pre-compressed springs for energy balancing systems has been presented. The proposed negative stiffness device is designed to have the capability for passively balancing the actuation requirement of systems displaying positive stiffness. The motivation for using such a mechanism was presented and an analytical model was derived to introduce the operating principle. The kinematics of the BTNS mechanism was introduced and the conversion of the positive stiffness spring into a negative stiffness system through geometric reconfiguration was investigated. A case study investigated the feasibility to generate the negative stiffness property for such a design through a simple assembly of LEGO® bricks. The experimental results from this prototype model were compared to the corresponding prediction from the analysis and proved the negative stiffness concept is worthy of further engineering application. A practical scenario was then considered to show the efficacy of the passive energy balancing concept by using a BTNS mechanism. An active camber mechanism used as the target load system, which has the capability for large, continuous changes in airfoil camber from the corresponding required torque input. The integrated BTNS mechanism was then considered to tailor the kinematics of the required torque driving the active camber and the results showed a similar torque-rotation profile can be generated. The BTNS mechanism has been numerically shown to reduce actuation torque requirement by 90% and increase the energy efficiency by at least 70%, allowing for smaller, lighter and lower cost actuators. Furthermore, optimisation allows for a higher energy efficiency to reduce further the actuation torque requirement. The design and testing of a demonstrator were shown, and the experimental results from this demonstrator were compared to the predictions from the analysis. The BTNS concept shown here can be extended to many potential actuation design applications which need frequent state switching to reduce the mean power consumption and waste heat dissipation.

Conflict of interest statement
Authors have no conflict of interest.

References

[1]   M.J. French, M.B. Widden, The spring-and-lever balancing mechanism, George Carwardine and the Anglepoise lamp, Proc. Inst. Mech. Eng. Part C J. Mech. Eng. Sci. 214 (2000) 501–508. doi:10.1243/0954406001523137.

[2]   R. Barents, M. Schenk, W.D. van Dorsser, B.M. Wisse, J.L. Herder, Spring-to-Spring Balancing as Energy-Free Adjustment Method in Gravity Equilibrators, in: Vol. 7 33rd Mech. Robot. Conf. Parts A B, 2009: pp. 689–700. doi:10.1115/DETC2009-86770.

[3]   Y.-L. Chu, C.-H. Kuo, A Single-Degree-of-Freedom Self-Regulated Gravity Balancer for Adjustable Payload [1], J. Mech. Robot. 9 (2017) 021006. doi:10.1115/1.4035561.

[4]   C.R. McInnes, D.G. Gorman, M.P. Cartmell, Enhanced vibrational energy harvesting using nonlinear stochastic resonance, J. Sound Vib. 318 (2008) 655–662. doi:10.1016/j.jsv.2008.07.017.

[5]   D.M. Correa, C.C. Seepersad, M.R. Haberman, Mechanical design of negative stiffness honeycomb materials, Integr. Mater. Manuf. Innov. 4 (2015) 10. doi:10.1186/s40192-015-0038-8.

[6]   K. Hoetmer, G. Woo, C. Kim, J. Herder, Negative Stiffness Building Blocks for Statically Balanced Compliant Mechanisms: Design and Testing, J. Mech. Robot. 2 (2010) 041007.

doi:10.1115/1.4002247.

[7]   C.B. Churchill, D.W. Shahan, S.P. Smith, A.C. Keefe, G.P. McKnight, Dynamically variable negative stiffness structures, Sci. Adv. 2 (2016) e1500778–e1500778. doi:10.1126/sciadv.1500778.

[8]   H. Kalathur, R. Lakes, Enhancement in piezoelectric sensitivity via negative structural stiffness, J. Intell. Mater. Syst. Struct. 27 (2016) 2568–2573. doi:10.1177/1045389X15624802.

[9]   W. Dong, F. Chen, M. Yang, Z.-J. Du, J. Tang, D. Zhang, Development of a highly efficient bridge-type mechanism based on negative stiffness, Smart Mater. Struct. 26 (2017). doi:10.1088/1361-665X/aa8102.

[10]   D.J. Clingman, R.T. Ruggeri, Mechanical strain energy shuttle for aircraft morphing via wing twist or structural deformation, in: E.H. Anderson (Ed.), Proc. SPIE Smart Struct. Mater. 2004 Ind. Commer. Appl. Smart Struct. Technol., San Diego, CA, 2004: p. 288. doi:10.1117/12.538681.

[11]   I.Y. Kwon, H.T.Y. Yang, P.K. Hansma, C.J. Randall, Implementable Bio-Inspired Passive Negative Spring Actuator for Full-Scale Structural Control under Seismic Excitation, J. Struct. Eng. 142 (2015) 04015079. doi:10.1061/(ASCE)ST.1943-541X.0001323.

[12]   B.K. Woods, M.I. Friswell, Spiral pulley negative stiffness mechanism for passive energy balancing, J. Intell. Mater. Syst. Struct. 27 (2016) 1673–1686. doi:10.1177/1045389X15600904.

[13]   B. Yang, Y. Guan, S. Wang, Q. Zou, X. Chu, H. Xue, A New Hybrid Gyroscope with Electrostatic Negative Stiffness Tuning, Sensors. 13 (2013) 7121–7139. doi:10.3390/s130607121.

[14]   A. Carrella, M.J. Brennan, T.P. Waters, K. Shin, On the design of a high-static-low-dynamic stiffness isolator using linear mechanical springs and magnets, J. Sound Vib. 315 (2008) 712–720. doi:10.1016/j.jsv.2008.01.046.

[15]   Y.C. Wang, R.S. Lakes, Extreme stiffness systems due to negative stiffness elements, Am. J. Phys. 72 (2004) 40–50. doi:10.1119/1.1619140.

[16]   Y. Liu, D.P. Yu, J. Yao, Design of an adjustable cam based constant force mechanism, Mech. Mach. Theory. 103 (2016) 85–97. doi:10.1016/j.mechmachtheory.2016.04.014.

[17]   R.A. Bos, D.H. Plettenburg, Design of a cosmetic glove stiffness compensation mechanism for toddler-sized hand prostheses, PLoS One. 12 (2017). doi:10.1371/journal.pone.0183233.

[18]   K. Hoetmer, J.L. Herder, C.J. Kim, A Building Block Approach for the Design of Statically Balanced Compliant Mechanisms, in: Vol. 7 33rd Mech. Robot. Conf. Parts A B, ASME, 2009: pp. 313–323. doi:10.1115/DETC2009-87451.

[19]   B.K.S. Woods, M.I. Friswell, N.M. Wereley, Advanced Kinematic Tailoring for Morphing Aircraft Actuation, AIAA J. 52 (2014) 788–798. doi:10.2514/1.J052808.

[20]   G. Radaelli, R. Buskermolen, R. Barents, J.L. Herder, Static balancing of an inverted pendulum with prestressed torsion bars, Mech. Mach. Theory. 108 (2017) 14–26. doi:10.1016/j.mechmachtheory.2016.10.005.

[21]   G.H. Yoon, J.S. Mo, Tailoring a bidirectional negative stiffness (BNS) structure with mechanical diodes for mechanical metamaterial structures, Smart Mater. Struct. 26 (2017). doi:10.1088/1361-665X/aa65bf.

[22]   P. Limaye, G. Ramu, S. Pamulapati, G.K. Ananthasuresh, A compliant mechanism kit with

flexible beams and connectors along with analysis and optimal synthesis procedures, Mech. Mach. Theory. 49 (2012) 21–39. doi:10.1016/j.mechmachtheory.2011.07.008.

[23] Y. Chen, J. Feng, Y. Liu, A group-theoretic approach to the mobility and kinematic of symmetric over-constrained structures, Mech. Mach. Theory. 105 (2016) 91–107. doi:10.1016/j.mechmachtheory.2016.06.004.

[24] K. V. Gothelf, LEGO-like DNA structures, Science (80-.). 338 (2012) 1159–1160. doi:10.1126/science.1229960.

[25] P. Celli, S. Gonella, Manipulating waves with LEGO®bricks: A versatile experimental platform for metamaterial architectures, Appl. Phys. Lett. 107 (2015). doi:10.1063/1.4929566.

[26] B.G. -g. Chen, N. Upadhyaya, V. Vitelli, Nonlinear conduction via solitons in a topological mechanical insulator, Proc. Natl. Acad. Sci. 111 (2014) 13004–13009. doi:10.1073/pnas.1405969111.

[27] B.K.S. Woods, M.I. Friswell, The Adaptive Aspect Ratio morphing wing: Design concept and low fidelity skin optimization, Aerosp. Sci. Technol. (2015). doi:10.1016/j.ast.2015.01.012.

[28] B.K.S. Woods, I. Dayyani, M.I. Friswell, Fluid/Structure-Interaction Analysis of the Fish-Bone-Active-Camber Morphing Concept, J. Aircr. 52 (2015) 307–319. doi:10.2514/1.C032725.

[29] B.K. Woods, O. Bilgen, M.I. Friswell, Wind tunnel testing of the fish bone active camber morphing concept, J. Intell. Mater. Syst. Struct. 25 (2014) 772–785. doi:10.1177/1045389X14521700.